Experimental Validation of a Laser Pulse Time-History Model

Fraser Dalgleish, Frank Caimi, Yueting Wan, Walter Britton
Florida Atlantic University/Harbor Branch Oceanographic Institute, 5600 US 1 North, Ft. Pierce, Florida 34946, USA

Joseph J. Shirron, Thomas E. Giddings
Metron, Inc.,11911 Freedom Drive, Suite 800, Reston, VA 20190-5602, USA

Charles H. Mazel, James M. Glynn, Jonathan P. Towle
Physical Sciences Inc., 20 New England Business Center, Andover, MA 01810, USA

INTRODUCTION

We are conducting equipment development, experimental, and computational work in support of a prototype pulsed laser line scan (PLLS) imaging system. Use of a pulsed rather than CW laser creates the potential for gating the return to reduce backscatter and increase signal-to-noise ratio, and for determining the range to each pixel to assemble a 3-D representation of the scene. The pulsed laser in combination with novel beam scanning and detection optics are being tested at a large purpose-built imaging test tank facility at the Florida Atlantic University/Harbor Branch Oceanographic Institute campus. A computational model (Giddings & Shirron, 2008) that incorporates both system hardware and water optical property parameters has been developed to aid in performance prediction and evaluation of alternative design parameters. The model evaluates the contributions from both volume backscatter and target reflections to predict the photon flux arriving at the receiver as a function of time. The model includes the option to use either a semi-analytical small-angle scattering approximation or a Monte Carlo code.

We conducted a series of experiments in the imaging test facility to validate the performance of the computational model. The pulsed laser operates at a wavelength of 532 nm at a 357 kHz repetition rate with 7 ns full width half maximum (FWHM) pulse width. Scattering was varied by the addition of Maalox and optical properties were measured with a WET Labs ac-9 meter. Parameters such as receiver aperture, source receiver separation, the pointing angle of the receiver and the turbidity of the water were systematically varied and a series of pulse time histories were recorded at a 5 GHz sampling rate for each set of conditions. The measured and modeled results were then compared. Discrepancies were evaluated to determine if the issue lay with the model or with the experiment. The model is proving to be a good predictor of pulse behavior, and the validation effort supports its use as a design tool for the development of the PLLS imaging system.

METHODS

A diagram of the experimental arrangement for the time-history measurements is shown in Figure 1. The laser source and the receiver were mounted on an optical table, 41 cm from the viewport. The receiver assembly was mounted on a precision computer-controlled rotation stage, and this in turn was mounted on a rail so that both the source-receiver (SR) separation and the receiver pointing angle could be adjusted. Precision apertures (1 and 3 mm) were placed at the focal point of the 50.8 mm (2 in.) receiver collection lens and a photomultiplier tube was positioned behind the iris so that the photocathode was 80% flooded when the 3mm aperture was used.

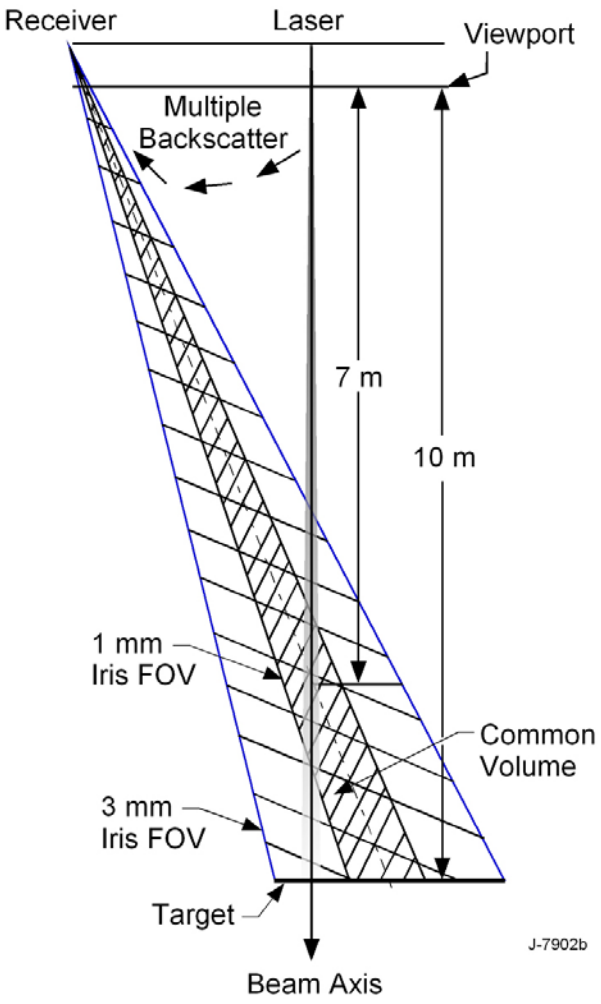

Figure 1. Schematic of the experimental arrangement for time-history measurements.

The laser source was a custom made system with a Nd:YVO_4 Q-switched oscillator followed by a solid state gain stage and an LBO frequency doubler. The laser produced 7 ns FWHM pulses at 532 nm at a 357 kHz repetition rate. A small portion of the output was sampled by a reference detector and used as a pulse monitor (to account for timing jitter in the laser pulse output) and for normalization of pulse-to-pulse amplitude variations.

Data were collected at SR separations of 83, 250, and 376 mm. At each SR separation the receiver was aligned so that the axis of the receiver field of view intersected the beam axis of the laser at 7 m from the viewport. Measurements were made at this central alignment, and at offsets from -6 to +6 mrad, in increments of 2 mrad, where a positive value corresponds to pointing the receiver at a shorter distance from the viewport.

A diffuse reflector target was positioned at 10 m from the viewport. The distinct return from the target served as a stable time reference, while not interfering with the common volume return.

The turbidity of the water in the tank was adjusted by adding or removing a 50/50 mixture of laboratory grade aluminum hydroxide and magnesium hydroxide powders, the scattering constituents

of Maalox. The commercially available antacid Maalox suspension contains additional non-scattering ingredients that make it more difficult to filter and can lead to algal growth. The powders were thoroughly mixed into fresh water and added into the path of the mixing jets in the test tank. Homogeneity of the measured beam attenuation coefficient (*c*) at different locations and depths within the tank was verified 30 - 40 minutes after addition. The particles varied between < 1μm and almost 100 μm, with the peak of the particle size distribution histogram around 5 μm. Absorption and attenuation were measured with a WET Labs ac-9 meter. Measurements were made at *c* values of 0.06, 0.25, 0.40, 0.48, and 0.63 m^{-1}.

In order to minimize alignment errors in the placement of the aperture in front of the receiver optics, the full set of measurements at the various SR separations, turbidities, and pointing angles were first made with the 1 mm aperture in place. The Maalox was then filtered from the tank in a 12 hour turnaround time, the 3 mm aperture was put in place, correct alignment was verified at each SR separation and the measurement sequence was repeated. The result was a total of 210 data sets (2 apertures, 3 SR separations, 7 pointing angles, and 5 turbidities).

Prior to running the pulse time-history experiments the beam spread function was measured by precisely micro-stepping the laser beam across the face of a wide angle of view, narrow spatial aperture radiometer with nine decades of linear measurement dynamic range. The results supported the use of the NAVAIR Maalox phase function in the models. (Laux et al., 2002)

TIME-DEPENDENT BACKSCATTER MODEL

The underwater lidar model calculates the time-dependent return due to volume backscatter and surface reflections in the object plane (Giddings & Shirron, 2008). The model conceives of a source that produces a narrow, pulsed beam, and a focused receiver aperture that is generally displaced from the source and whose field-of-view is canted at a small angle to align with the source axis in the object plane. The source radiance and the spatio-angular response pattern of the receiver aperture may be non-axisymmetric. In general, the optical properties of the medium vary in the direction of beam propagation. The model first computes the temporal impulse response for the system in the prescribed environment. This impulse response is then convolved with the output pulse shape to obtain the received signal.

The optical paths are limited to multiple small-angle forward scattering and a single large-angle scattering event in the backward direction (DeWolf, 1971). The numerical formulation discretizes the optical medium into "slabs" of finite thickness (*dz*) lying perpendicular to the direction of beam propagation. The return from each slab is treated in much the same way as the return from a flat, solid surface; that is, by convolving the system's spatial impulse response with the uniform reflectivity of the slab. The spatial impulse response is computed based on the solution to the radiative transfer equation under the small-angle scattering approximation (RTE/SAA), as described by Dolin (1964), and with no further simplifying assumptions. The flux reflectance of a slab at distance *z* along the beam axis is $R = \pi\, dz\, \beta_\pi(z)$, where β_π is the backscatter coefficient.

We employ a semi-analytical approach that reduces the general problem for each slab to at most a few one-dimensional integrals. In the special case of axisymmetric apertures this problem reduces to a single one-dimensional integral in accord with the developments in Mertens & Replogle (1977) and Korshunov (1980), for example. Conceptually, the model evaluated here has much in common with

models presented by Dolin & Saval'yev (1971), Mertens & Replogle (1977), Zege et al. (1995), Katsev et al. (1997), and Korshunov (1980). The main differences are that the present formulation uses the full RTE/SAA solutions and that the numerical approach greatly reduces the computational burden in the general, asymmetric aperture cases. The present model has been rigorously verified using Monte Carlo simulations and has shown excellent agreement in resolving the return from the multiple-scatter and common volume backscatter regions.

RESULTS

A typical laser pulse return through scattering media has three distinct components, as shown in Figure 2. Starting from time zero, the first broad return is due to multiple scattering (MS) from particles near the viewport, where the laser energy is greatest. This is followed by the narrower return from the common volume (CV), defined by the intersection of the receiver field-of-view with the laser beam. And, finally, we have the reflection from the target in the object plane. The CV return peak occurs close to the onset of the CV region since the intensity of the laser pulse falls off exponentially as it transits the CV. At higher turbidities the MS return is significant and overlaps the CV return, shifting the apparent position of the CV peak to the left on the time axis. In the discussion that follows we will consider the effect of changing each experimental variable on the MS and CV returns.

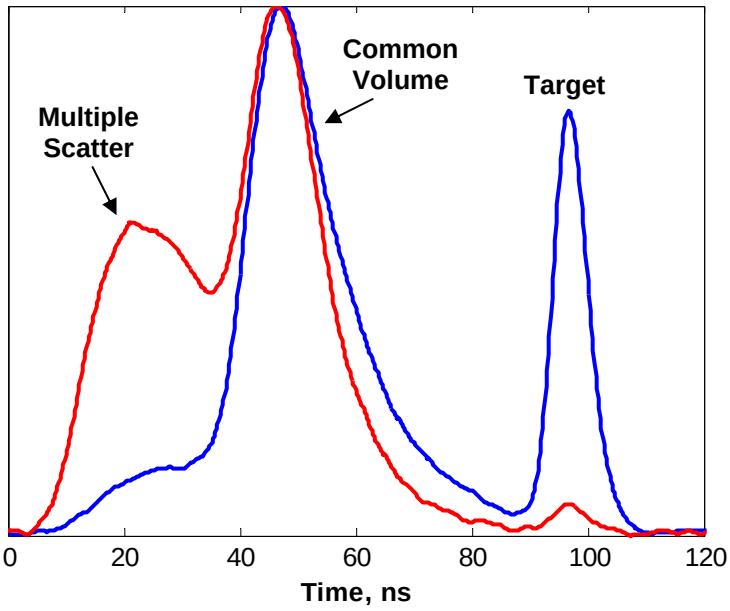

Figure 2. Representative normalized laser pulse time-history measurements for two turbidities. At the higher turbidity (red) the multiple scatter peak is stronger and the target return is weaker.

As we decrease the SR separation for a given aperture, pointing angle, and turbidity we expect the onset of both the MS and CV returns to begin sooner. See Fig. 3.

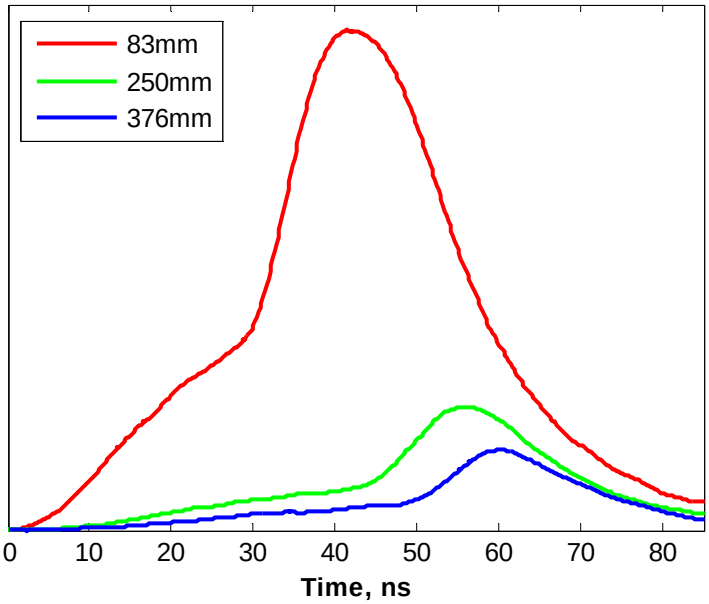

Figure 3. Time-history returns for source-receiver separation of 83 mm (red), 250 mm (green) and 376 mm (blue). Receiver aperture = 3mm, c = 0.25 m^{-1}.

As we increase the aperture (from 1 to 3 mm) for a given SR separation, pointing angle, and turbidity we expect the onset of both the MS and CV returns to begin sooner, and for the amplitude to increase. See Fig. 4.

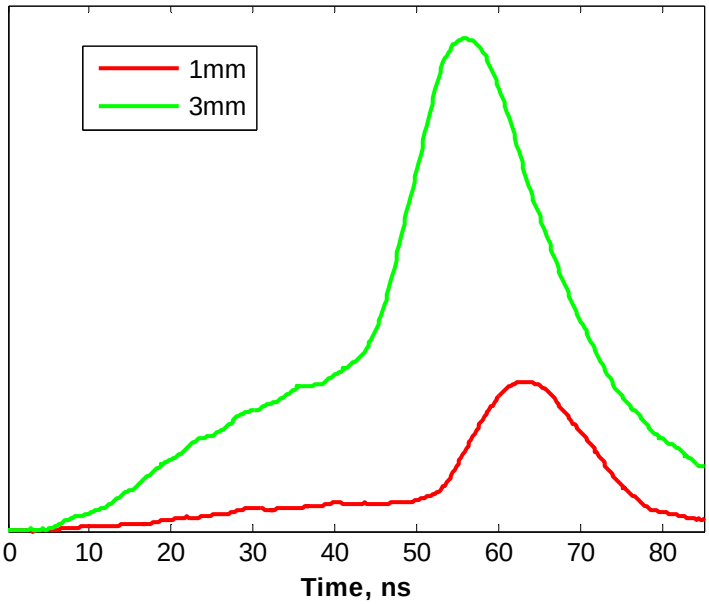

Figure 4. Time-history returns for receiver apertures of 1 mm (red) and 3 mm (green). Source-receiver separation 250mm, c = 0.25 m^{-1}, pointing angle = 0 mrad.

As we adjust the pointing angle from -6 to +6 mrad for a given aperture, SR separation, and turbidity we expect the onset of both the MS and CV returns to begin sooner, and for the amplitude to increase. See Fig. 5.

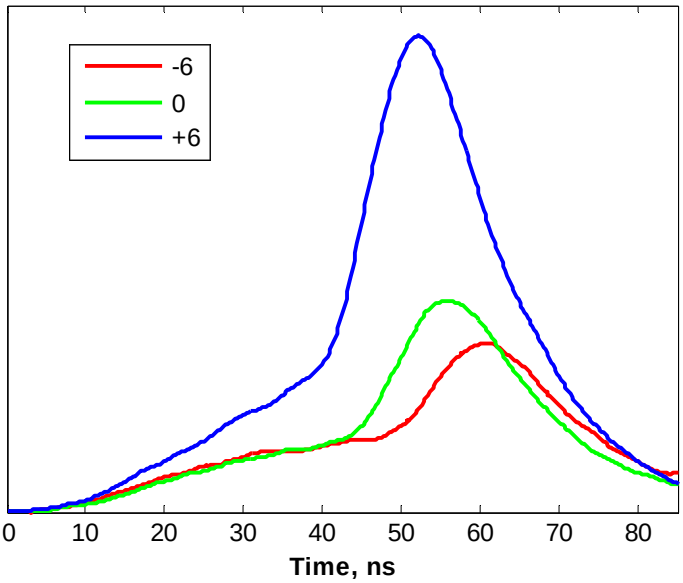

Figure 5. Time-history returns for receiver pointing angles of -6 (red), 0 (green) and +6 (blue) mrad. Source-receiver separation 250mm, c = 0.25 m^{-1}, receiver aperture = 3mm.

As we increase turbidity for a given aperture, SR separation, and pointing angle we expect the MS return to begin sooner and become larger. The CV return should not change in time and should decrease in strength, as more of the energy would have been removed from the beam before it entered the CV. See Fig. 6.

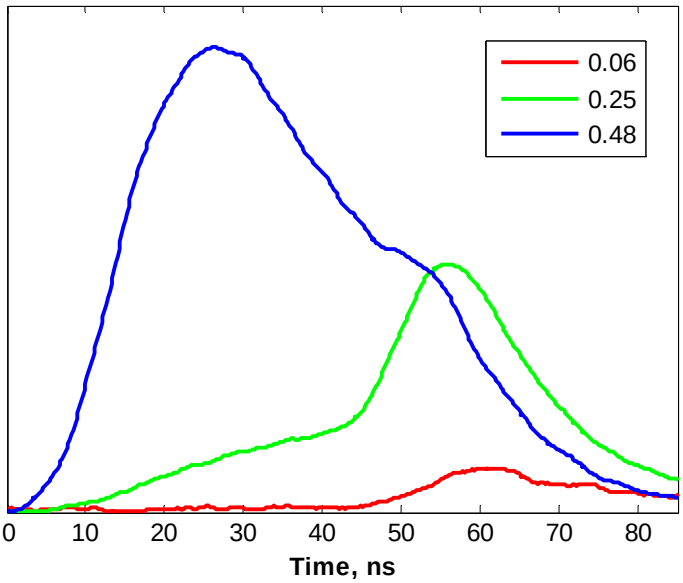

Figure 6. Time-history returns for turbidities of c=0.06 m^{-1} (red), 0.25 (green) and 0.48 (blue). Source-receiver separation 250mm, receiver aperture = 3mm.

MODEL COMPARISON

The agreement between the experiment and the model was quite good. A small selection of comparison graphs are shown in the following figures. The returns from the target are omitted.

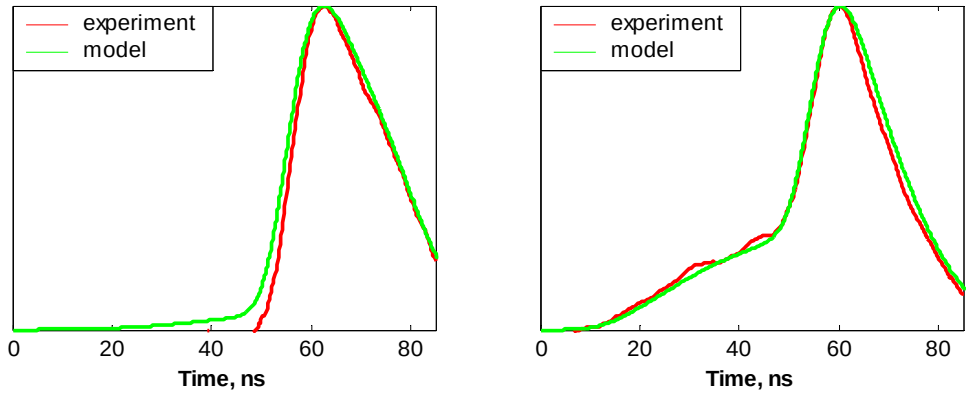

Figure 7. Graphs of the experimental data (red) and model results (green). Left: c=0.08m^{-1}, SR=376mm, aperture = 3mm. Right: c=0.25 m^{-1}, SR=376mm, aperture = 3mm.

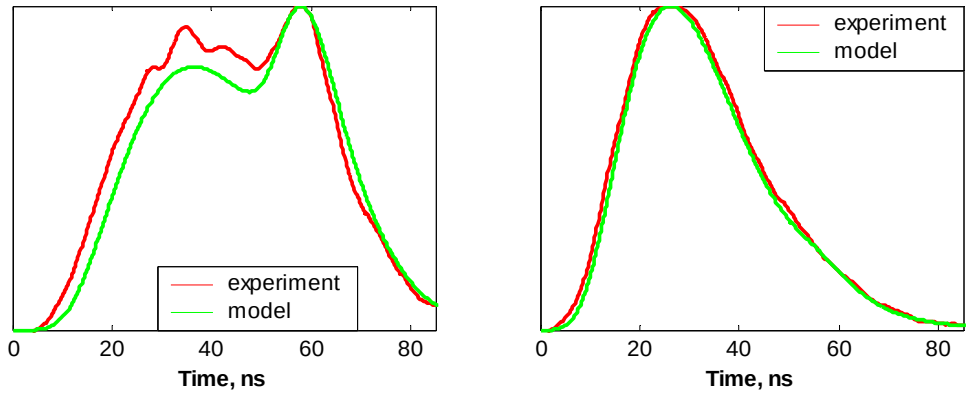

Figure 8. Graphs of the experimental data (red) and model results (green). Left: c=0.48 m^{-1}, SR=376mm, aperture = 3mm. Right: c=0.63 m^{-1}, SR=376mm, aperture = 3mm.

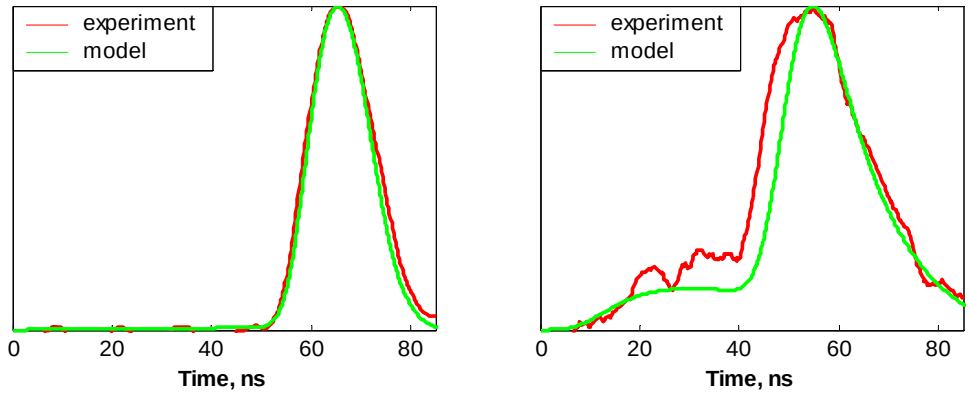

Figure 9. Graphs of the experimental data (red) and model results (green). Left: c=0.06 m^{-1}, SR=250mm, aperture = 1mm. Right: c=0.25 m^{-1}, SR=83mm, aperture = 1mm.

CONCLUSIONS

The experimental effort described here demonstrates that the new pulsed laser backscatter model is a good predictor of observed behavior. The results support its use as an analysis tool in the development and performance prediction for a pulsed laser line scan imager.

The larger-scale motivation for this work is to investigate the potential benefits of using a pulsed laser source with a gated detector to improve the performance of underwater laser line scan imaging systems relative to CW lasers and detectors. In particular this model can be used to predict the time history of backscatter peaks in water of different turbidities. This ability to predict the temporal position of backscatter peaks provides guidance for gating the detector of a PLLS system, thus improving the signal-to-noise ratio above that achievable with a CW LLS imaging system. The study presented here has provided validation for a time-history model that can be used in the development of future PLLS.

REFERENCES

DeWolf, D. A., 1971. “Electromagnetic reflection from an extended turbulent medium: Cumulative forward-scatter single-backscatter approximation,” IEEE Trans. Antennas Propogat. AP-19, 254–262.

Dolin, L. S., 1964. “Propagation of a narrow light beam in a random medium,” Izv. VUZ, Radiofizika 7, 380–382 (1964). (in Russian).

Dolin, L. S., and V. A. Savel’yev, 1971. “Backscattering signal in pulsed irradiation of a turbid medium with a narrow directional light beam,” Izv., Acad. Sci., USSR, Atmos. Oceanic Phys. 7, 328–331.

Giddings, T.E. and Shirron, J.J., 2008, Numerical Simulation of the Electro-Optical Imaging Process in Plane-Stratified Media, submitted to *Applied Optics*.

Katsev, I. L., E. P. Zege, A. S. Prikhach, and I. N. Polonsky, 1997. “Efficient technique to determine backscattered light power for various atmospheric and oceanic sounding and imaging systems,” J. Opt. Soc. Am. A 14, 1338–1346.

Korshunov, V. A., 1980. “Laser radar equation in the small-angle approximation,” Radiophys. Quantum Electron. 24, 748–755.

Laux, A., R. Billmers, L. Mullen, B. Concannon, J. Davis, J. Prentice, and V. Contarino, 2002. "The abc's of oceanographic lidar predictions: a significant step toward closing the loop between theory and experiment," J. Mod. Opt. 49, 439-451

Mertens, L. E., and F. S. Replogle, Jr., 1977. “Use of point spread and beam spread functions for analysis of imaging systems in water,” J. Opt. Soc. Am. 67, 1105–1117.

Zege, E. P., I. L. Katsev, and I. N. Polonsky, 1995. “Analytical solution to LIDAR return signals from clouds with regard to multiple scattering,” Appl. Phys. B 60, 345–353.